Research Article **Open Access**

Interaction of Fluorescent 2-(1-Methoxynaphthalen-4-Yl)-1-(4-Methoxyphenyl)-4, 5-Diphenyl-1H-Imidazole with Pristine Zno, Cu-Doped Zno and Ag-Doped Zno Nanoparticles

P Ponnambalam[1], S Kumar[1,2*] and P Ramanathan[3]

[1]Department of Chemistry, Bharathiar University, Coimbatore-641046, Tamilnadu, India
[2]Department of Chemistry, Thiruvalluvar College of Engineering and Technology, Tamilnadu, India
[3]Department of Chemistry, Thanthai Hans Roever College (Autonomous), Perambalur, Tamilnadu, India

Abstract

A sensitive 2-(1-methoxynaphthalen-4-yl)-1-(4-methoxyphenyl)-4, 5-diphenyl-1H-imidazole (MNMPI) fluorescent sensor for nanoparticulates like ZnO, Cu-doped ZnO and Ag-doped ZnO has been designed and synthesized. Facile preparation of ZnO, Cu-doped ZnO and Ag-doped ZnO nanoparticles by sol-gel method using PVP K-30 as templating agents is reported and characterised by powder X-ray diffraction (XRD), scanning electron microscopy (SEM), UV-Visible spectroscopy and photoluminescence spectroscopy (PL). The synthesized sensor release is enhanced by nanocrystalline pristine ZnO but is suppressed by Cu-doped ZnO and Ag-doped ZnO nanoparticles. The suppression of fluorescence is additional by copper than by silver doping. The LUMO and HOMO energy gap of MNMPI associated with Cu-doped ZnO are lowers compared to those of pristine ZnO and thus red shift compared to that with pristine ZnO. The average crystallite sizes of ZnO, Cu-doped ZnO and Ag-doped ZnO have been deduced as 32 nm, 36 nm and 26 nm and calculated surface area for ZnO, Cu-doped ZnO and Ag-doped ZnO are 30.04 m²/g, 40.66 m²/g and 29.37 m²/g respectively. The observed enhanced absorbance with the distributed semiconductor nanoparticle is due to adsorption of MNMPI on semiconductor surface. This is because of the efficient transfer of electron from the excited state of the MNMPI to the conduction band of the semiconductor nanoparticle.

Keywords: MNMPI; ZnO; Cu-doped ZnO; Ag-doped ZnO; XRD; SEM; UV; PL

Introduction

The report as Xia is for Polymer-stabilized nano ZnO with blue emission [1] and the cell imaging is obtained by tunable photoluminescence with and the ZnO@polymer core-shell nanoparticles [2,3]. Using single crystals or polycrystalline of Co²⁺: ZnO prepared by pellet sintering many scholars identified the observable photo response of Co-doped ZnO. They establish that the Ni-doped ZnO unfilled spheres exhibited only feeble ferromagnetism at 300 K whereas Co-doped ZnO hollow exhibited ferromagnetism at room temperature. Not due to any cobalt oxide phase formation or any metallic Co isolation the observed nature of ferromagnetism was intrinsic. Heterocyclic imidazole moieties have also attracted significant attention because of their unique optical properties [4] and for their use in preparing functionalized materials [5]. Nanoparticles can be used as drug carriers because they have enormous surface area and due to their submicron size they can efficiently be taken up by the cells [6]. ZnO is an attractive semiconductor material with wide direct band gap (3.37 eV), large exciton binding energy (60 meV) and a hexagonal structure and have significant applications in optoelectronics, sensors and actuators [7-9]. Hence, ZnO is one of the most attractive platforms for binding enzyme and shows potential material for a wide range of biosensor applications. Au, Ag, or Pt noble metal layered ZnO is significant for photoelectron transfer (PET) in the bulk and interface of ZnO semiconductors [10]. Under clarification of UV light, the exciton absorption bands of ZnO are strongly bleached due to the accumulation of conduction band electrons [11]. Thus, the effectiveness of both the photocatalysis and photoelectric energy conversion can be significantly enhanced by depositing noble metals on the surface of ZnO [12]. The properties and applications of noble metal ZnO nanostructured materials are also determined by its morphology, structure and the organization of nanostructured ZnO architectures [13-16]. ZnO based various ceramics were synthesised by liquid phase sintering of ZnO powder of different sizes and morphologies. The HOMO and LUMO

potentials for the considered sensor must match with the conduction and valence band edges of the semiconductor nanocrystals [17].

Experimental

Materials and methods

Benzil, 4-methoxyaniline, 4-methoxynaphthaldehyde, ammonium acetate and borontrifluoride ethylethartate were purchased from Sigma Aldrich. Zinc acetate (Sd fine), polyvinylpyrrolidone (PVP K-30, Himedia), ammonia (Qualigens). The solvents used for spectral measurements were of spectroscopic grade and purchased by Hi-media. Distilled ethanol and deionized distilled water were employed for the experiments.

Synthesis 2-(1-methoxynaphthalen-4-yl)-1-(4-methoxyphenyl)-4, 5-diphenyl-1H-imidazole

The product 2-(1-methoxynaphthalen-4-yl)-1-(4-methoxy phenyl)-4, 5-diphenyl-1H-imidazole was prepared by refluxing benzil (1 mmol), 4-methoxyaniline (1 mmol), 4-methoxynaphthaldehyde (1 mmol) and ammonium acetate (1 mmol) in ethanol (20 mL) for 2 h, borontrifluoride ethylethartate (1 mol%) acting as a catalyst (Scheme-1). The progress of the reaction was followed by TLC. After completion of the reaction, the mixture was cooled, dissolved in acetone and filtered. The product was

purified by column chromatography with benzene: ethyl acetate (9:1) as the eluent.

M.P. 296°C. Anal. calcd. for $C_{33}H_{26}N_2O_2$: C, 82.13; H, 5.43; N, 5.81. Found: C, 82.11; H, 5.41; N, 5.80. ^{1}H NMR (400 MHz, CDCl$_3$): δ 3.55 (s, 3H), 3.88 (s, 3H), 6.44 (d, J=8.4 Hz, 2H), 6.62 (d, J=8.0 Hz, 1H), 6.73 (d, J=8.4 Hz, 2H), 7.12-7.18 (m, 9H), 7.29-7.44 (m, 4H), 7.82 (dd, J=6.4 Hz, 1H), 8.13 (d, 1H). ^{13}C NMR (400 MHz, CDCl$_3$): δ 54.18, 54.57, 102.98, 112.76, 117.88, 121.03, 124.33, 124.34, 124.46, 125.91, 126.12, 126.55, 127.11, 127.17, 127.32, 127.46, 127.74, 127.78, 129.01, 129.28, 129.97, 132.14, 132.36, 135.40, 145.36, 155.39, 157.70. MS: m/z. 482.57 [M +].

Synthesis of nanocrystalline oxides by Sol-gel method

Zinc nitrate (0.1 g) solution [with or without Cu(NO$_3$)$_2$/AgNO$_3$] in 10 ml 0.01 M PVP K-30, newly prepared solution of 1:1 aq. NH$_3$ was added slowly to reach a pH of 7, under continuous stirring. The stirring was sustained for another 30 min to get a gel. The formed glassy like white gel was allowed to age overnight. It was filtered and washed with water and ethanol several times, dried at 100°C for 12 h and calcinated at 500°C for 3 h to pale grey solid.

Spectral measurements

The ^{1}H NMR and proton decoupled ^{13}C NMR spectra were recorded to using a Bruker 400 MHz NMR spectrometer operating at 400 MHz and 100 MHz, respectively. The UV-vis absorption and emission spectra were recorded with PerkinElmer Lambda 35 spectrophotometer and PerkinElmer LS55 spectrofluorimeter, respectively. The powder X-ray diffractogram (XRD) was recorded with a PAN analytical X'Pert PRO diffractometer using Cu Kα rays at 1.5406 Å with a tube current of 30 mA at 40 kV. A JEOL JSM 10LV scanning electron microscope (SEM) equipped with a highly sensitive backscattered detector and low vacuum secondary detector was used to get the SEM image of the sample. The UV-vis absorption spectra were recorded with PerkinElmer Lambda 35 spectrophotometer.
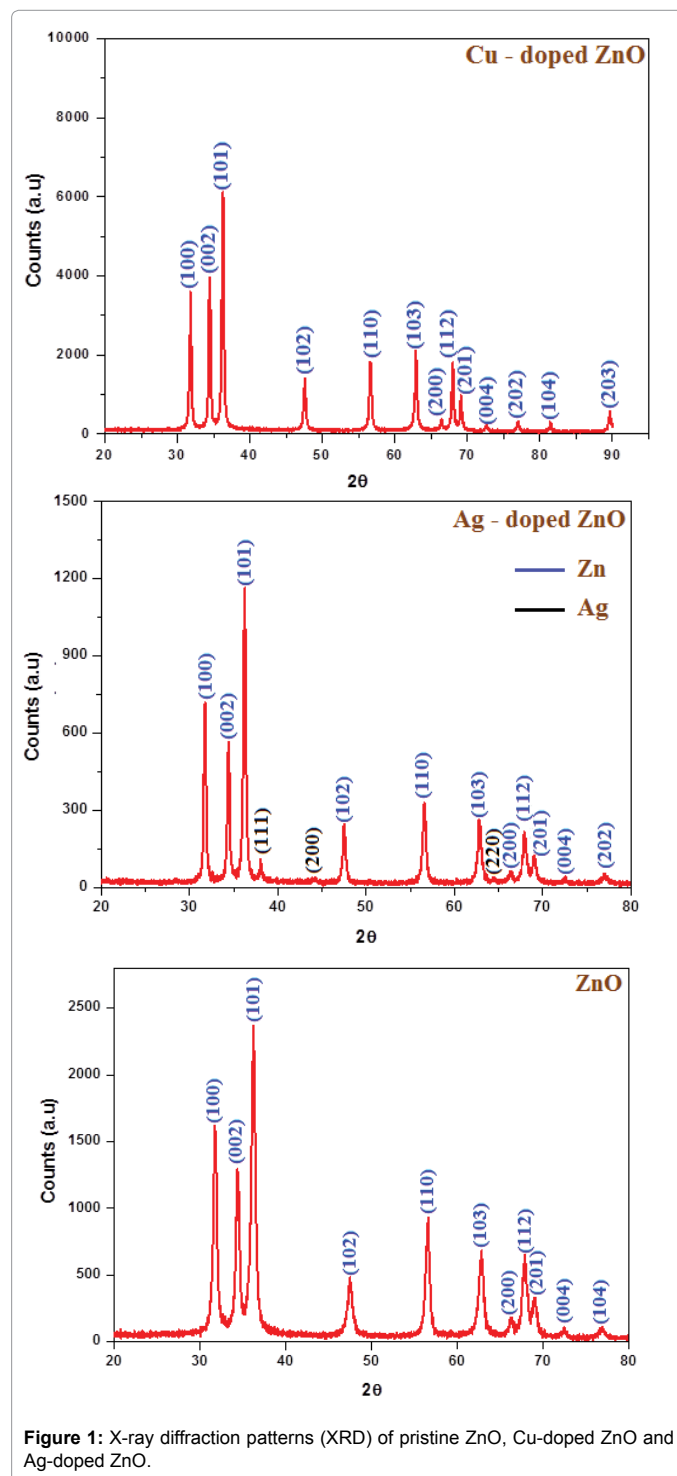
Results and Discussion

XRD analysis of ZnO, Cu-doped ZnO and Ag-doped ZnO nanoparticles

X-ray diffraction patterns (XRD) of pristine ZnO, Cu-doped ZnO and Ag-doped ZnO nanoparticles obtained by sol-gel method (Figure 1). All the diffraction patterns match with the JCPDS pattern of Zincite
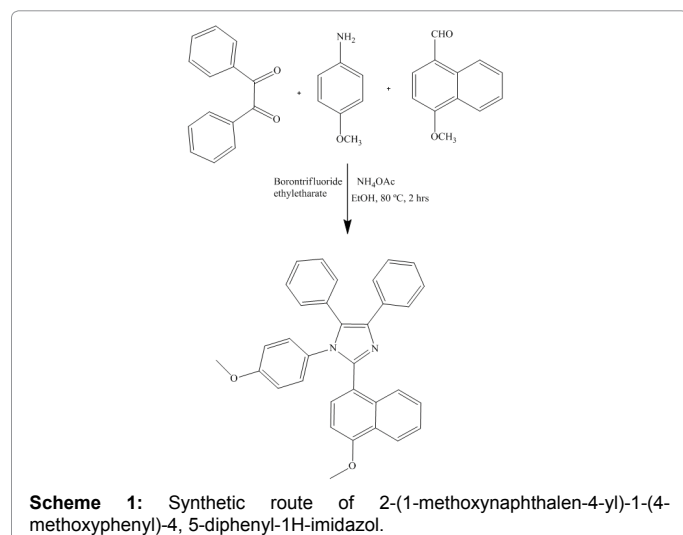
(89-7102). The crystal structures of pristine ZnO and doped ZnO are primitive hexagonal with crystal constants a and b as 3.249 A° and c as 5.025 A°. In the case of doping with copper, as the radii of Zn^{2+} and Cu^{2+} are comparable, Cu^{2+} can replace Zn^{2+} in the lattice without change in the lattice parameters. The XRD of Ag-doped ZnO reveals the presence of metallic silver in face centered crystal lattice whereas the Cu-doped ZnO fails to provide any peak other than those of ZnO. The observed peak at 38.2° is characteristic of the 111-peak of face centered cubic phase of metallic silver. The Ag$^+$ ion is better (radius 1.22 A°) than that of Zn^{2+} (0.72 A°) and hence cannot be included in to the ZnO lattice.

Figure 1: X-ray diffraction patterns (XRD) of pristine ZnO, Cu-doped ZnO and Ag-doped ZnO.

Scheme 1: Synthetic route of 2-(1-methoxynaphthalen-4-yl)-1-(4-methoxyphenyl)-4, 5-diphenyl-1H-imidazol.

Hence silver preferentially desire to segregate around the ZnO grain boundaries. The average crystallite sizes (L) of the sol-gel synthesized ZnO, Cu-doped ZnO and Ag-doped ZnO have been deduced as 32 nm, 36 nm and 26 nm, respectively. They have been obtained from the full width at half maximum (FWHM) of the most intense peaks of the individual crystals using the Scherrer equation, $L = 0.9\ \lambda/\beta\cos\theta$, where λ is the wavelength of the X-rays used, θ is the diffraction angle and β is the full width at half maximum of the peak. The calculated surface area for ZnO, Cu-doped ZnO and Ag-doped ZnO are 30.04 m²/g, 40.66 m²/g and 29.37 m²/g, respectively.

SEM and EDS analysis of ZnO, Cu-doped ZnO, Ag-doped ZnO nanoparticles and imidazole-ZnO complex

The SEM images of pristine ZnO, Cu-doped ZnO and Ag-doped ZnO nanoparticles are displayed in Figure 2. The particles are flower like use of PVP as templating agent provides finite morphology. The EDS spectra are shown in Figure 3 confirm the existence of zinc, oxygen, copper and silver signals which implies the purity of the synthesized ZnO and Cu-doped ZnO nanoparticles.

Absorption and emission behaviours of imidazole with ZnO, Cu-doped ZnO, Ag-doped ZnO nanoparticles

The photoluminescence spectra of pristine ZnO, Cu-doped ZnO and Ag-doped ZnO nanoparticles have been recorded at room temperature. They are shown in Figure 4. The pristine ZnO, Cu-doped ZnO and Ag-doped ZnO nanoparticles exhibit near band gap emission (NBE) and deep level emission (DLE). The DLE arises due to different intrinsic and extrinsic structural defects in all the nanoparticles [18]. The NBE originates from the recombination of free photogenerated electrons and holes. These UV emissions concur with the absorption edges deduced from the Kubelka-Munk plots. Pristine ZnO display the emission around 418 nm was observed [19,20]. The emission originates from the electron transition from the superficial donor level of oxygen vacancies to the valence band (VB) and electron transition from the superficial donor level of zinc interstitials to the VB [21]. This emission energy corresponds to the electron change from deep-level donor of the

ionized oxygen vacancies to the VB. The absorption spectra of MNMPI in the existence of pristine ZnO, Cu-doped ZnO and Ag-doped ZnO nanoparticles distributed at different loading and also in their absence are displayed in Figure 5. The nanoparticles enhance the absorbance of MNMPI remarkably. The observed enhanced absorbance with the distributed semiconductor nanoparticle is due to adsorption of MNMPI on semiconductor surface. This is because of the efficient transfer of electron from the excited state of the MNMPI to the conduction band of the semiconductor nanoparticle. The emission spectra of MNMPI in the existence of pristine ZnO, Cu-doped ZnO and Ag-doped ZnO nanoparticles distributed at different loading and also in their absence are displayed in Figure 4. The pristine ZnO nanoparticle enhances the emission of MNMPI. The enhanced emission with the dispersed semiconductor nanoparticles is due to the adsorption of MNMPI on semiconductor surface. Fluorescence enhancement is due to the formation of complex [MNMPI-nanoparticulate ZnO]. Doping of ZnO by Ag and Cu shows that the dopants inhibit the fluorescence enhancement by ZnO. Figure 6 shows the linear variation of log $[F_0\text{-}F/F_0]$ vs. [nanoparticles] and the calculated binding constant (K) is given in Table 1. The order of binding constant (K) is Cu-doped ZnO>ZnO>Ag-doped ZnO. The binding constant (K) of the imidazole with ZnO and Cu-doped ZnO are in the order of 10^7 whereas that with
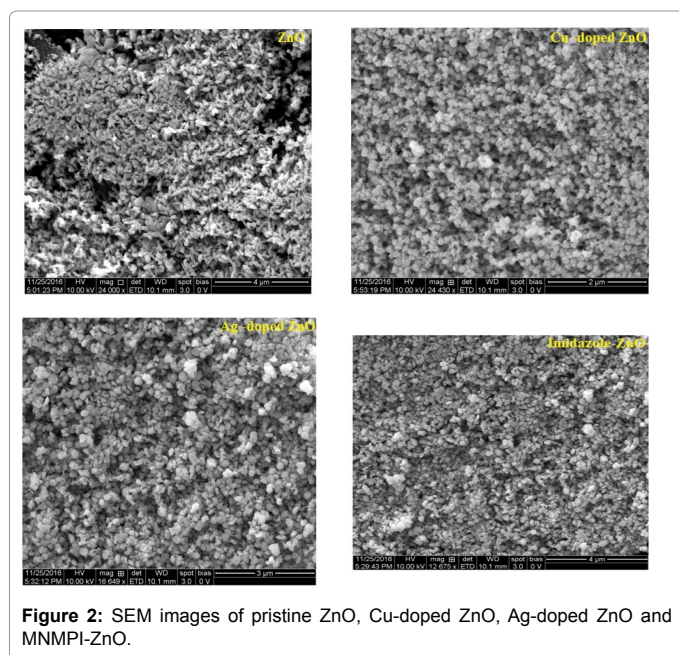

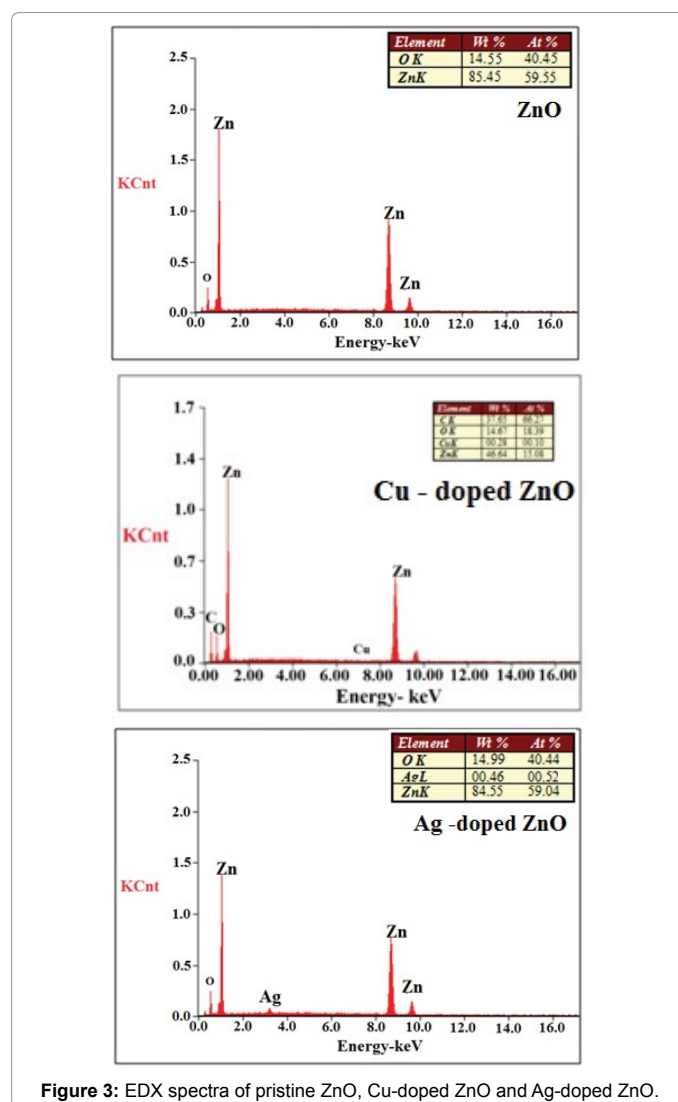**Figure 2:** SEM images of pristine ZnO, Cu-doped ZnO, Ag-doped ZnO and MNMPI-ZnO.

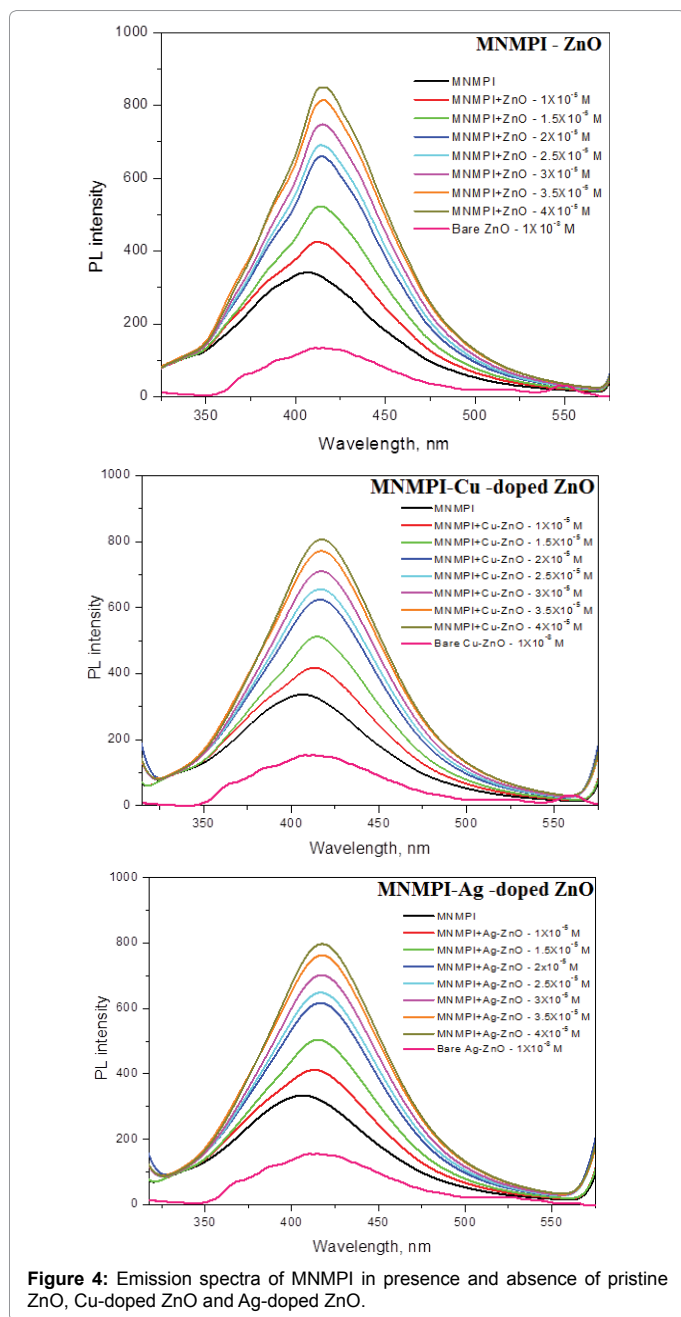**Figure 3:** EDX spectra of pristine ZnO, Cu-doped ZnO and Ag-doped ZnO.

Figure 4: Emission spectra of MNMPI in presence and absence of pristine ZnO, Cu-doped ZnO and Ag-doped ZnO.

levels have been calculated using the equations [21], HOMO=-e $(E_{ox}+4.71)$ (eV); LUMO=-e $(E_{red}+4.71)$ (eV). On the origin of the relative HOMO and LUMO energy levels of an inaccessible MNMPI molecule along with the conduction band and valence band edges of

Complex	τ	k_r	k_{nr}	K	n
MNMPI	3.72	0.80	1.9	-	-
MNMPI... ZnO	3.33	0.90	2.1	2.98×10^8	0.97
MNMPI... Cu-ZnO	3.21	0.69	2.6	9.89×10^9	0.98
MNMPI... Ag-ZnO	3.42	0.79	2.2	9.02×10^7	0.91

Table 1: Photoluminescence (τ, ns), radiative (k_r, $10^8 s^{-1}$), non-radiative (k_{nr}, $10^8 s^{-1}$), binding constant (K), binding sites (n).
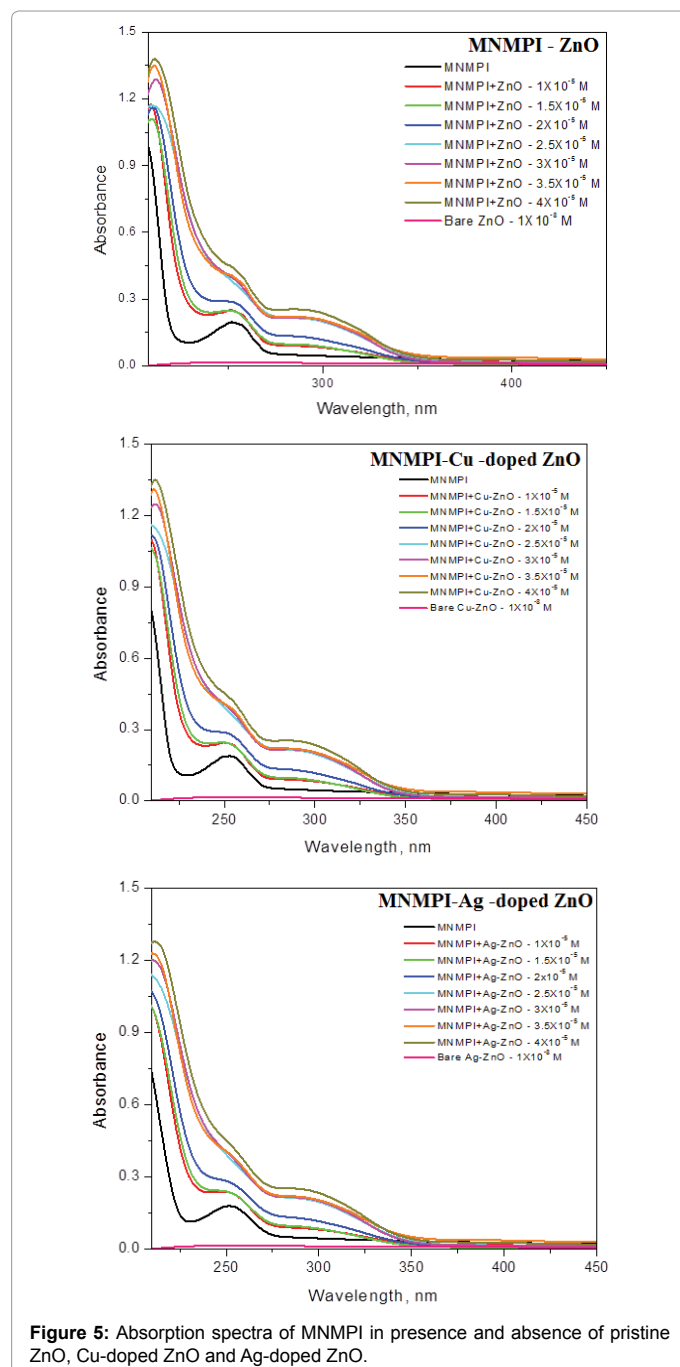

Figure 5: Absorption spectra of MNMPI in presence and absence of pristine ZnO, Cu-doped ZnO and Ag-doped ZnO.

Ag-doped ZnO is far less. This is because in Ag-doped ZnO, Ag^0 is deposited on the surface of the crystal thereby inhibiting the binding of the imidazole with ZnO. In Cu-doped ZnO, Cu^{2+} is likely to be present in the cationic sites or the interstitial positions thereby not influence the binding of imidazole with ZnO. Both the dopants suppress the enhancement of fluorescence and the inhibition is more by copper than by silver doping. The possible reason is Cu^{2+} in Cu-doped ZnO may bind with the imidazole and this binding could be much stronger than that by Zn^{2+}. The binding of Ag with imidazole is not as strong as that of Cu^{2+} or Zn^{2+} and thus less binding constant.

HOMO-LUMO energy levels of imidazole with ZnO, Cu-doped ZnO, and Ag-doped ZnO nanoparticles

From the onset oxidation potential (E_{ox}) and the onset reduction potential (E_{red}) of MNMPI derivative, HOMO and LUMO energy

Figure 6: Stern-Volmer plot of log $[F_0\text{-}F/F_0]$ vs. [nanoparticles].

nanocrystals is also possible because the electron in the LUMO of the excited imidazole is of higher energy compared to that in the CB of ZnO nanocrystals [22]. This should lead to quenching of fluorescence of MNMPI. However, in differing to the expectations, enhancement of fluorescence is observed in the presence of ZnO nanocrystals. This may be because of lowering of the HOMO and LUMO energy levels of MNMPI due to adsorption on ZnO nanoparticles. The polar ZnO covering enhances the delocalisation of the π electrons and lowers the HOMO and LUMO energy levels due to adsorption. The chemical

Figure 7: HOMO and LUMO energy levels of MNMPI along with the CB and VB edges of pristine ZnO, Cu-doped ZnO and Ag-doped ZnO.

Figure 8: Schematic diagram describing the photoelectron transfer from MNMPI to nanoparticles.
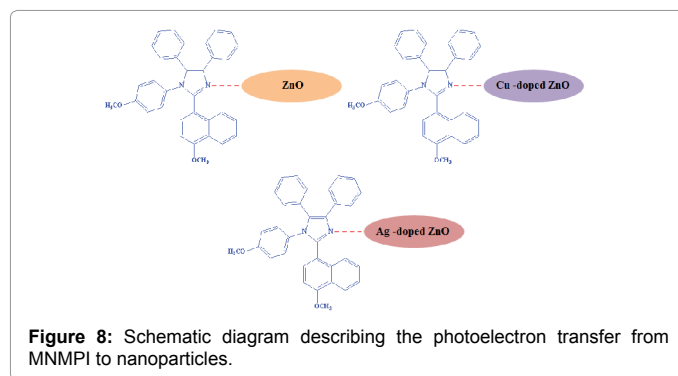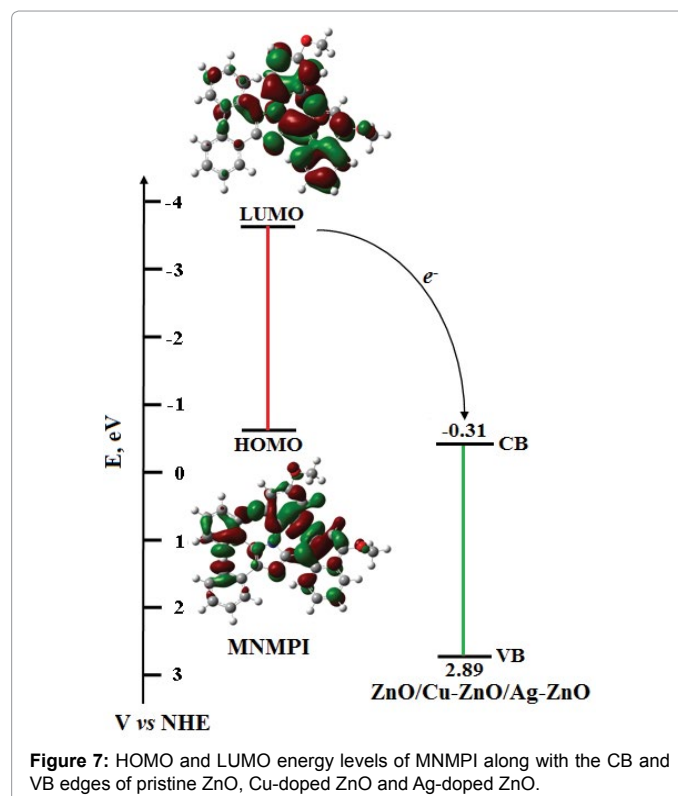
affinity between the nitrogen atom of the imidazole and zinc ion on the surface of the nano-oxide may be a reason for strong adsorption of the imidazole on nanoparticle causes the enhancement.

Binding interaction of imidazole with ZnO, Cu-doped ZnO, Ag-doped ZnO nanoparticles

The binding strength of MNMPI through its azomethine nitrogen with Cu^{2+} in the doped ZnO is likely to be stronger than that with Zn^{2+} in pristine ZnO (Figure 8). The LUMO and HOMO energy gap of

ZnO nanoparticles as shown in Figure 7, the electron injection would be thermodynamically allowed from the excited singlet of the MNMPI derivative to the conduction band of ZnO. The energy levels presented in Figure 7 reveals the enhancement of fluorescence of MNMPI by ZnO nanocrystals. Electron transfer from the excited imidazole to the

MNMPI associated with Cu-doped ZnO are lowers compared to those of pristine ZnO. This inference stems from the observed red shift of the fluorescence of MNMPI on binding with Cu^{2+}-doped ZnO compared to that with pristine ZnO. The emission of MNMPI is blue shifted on association with Ag-doped ZnO. The doped silver is likely to be present as metallic silver nano deposit on the surface of ZnO nanoparticles. The metallic silver on the surface of ZnO nanoparticles is likely to interrelate with MNMPI through its azomethine nitrogen. The interaction is likely to be weak as Ag^0 is involved instead of its ionic form. The deposited silver on the surface of ZnO nanocrystals act as a shield making the MNMPI-Zn^{2+} of ZnO interaction less possible. The energy gap between HOMO and LUMO of the MNMPI-Ag-doped ZnO becomes larger compared to that with complex MNMPI-ZnO.

Conclusion

In conclusion, a sensitive MNMPI fluorescent sensor for nanoparticulate ZnO has been designed and synthesized. Facile preparation of ZnO, Cu-doped ZnO and Ag-doped ZnO nanoparticles by sol-gel method using PVP K-30 as templating agents is reported and characterised by X-ray diffraction, energy dispersive X-ray, UV-visible diffuse reflectance and photoluminescence spectra. MNMPI is adsorbed on the surface of semiconductor nanoparticle during azomethine nitrogen. The polar ZnO surface enhances the delocalisation of the π electrons and lowers the HOMO and LUMO energy levels due to adsorption. The LUMO and HOMO energy gap of MNMPI associated with Cu-doped ZnO are lowers compared to those of pristine ZnO and thus red shift compared to that with pristine ZnO. The energy gap between HOMO and LUMO of the complex MNMPI-Ag-doped ZnO becomes larger compared to that with complex MNMPI-ZnO and the emission compared to those of pristine ZnO. The conduction band energy position determines the electron transfer from excited state MNMPI to the ZnO, Cu-doped ZnO and Ag-doped ZnO nanoparticles.

References

1. Xiong HM, Wang ZD, Xia YY (2006) Polymerization initiated by inherent free radicals on nanoparticle surfaces: A Simple method of obtaining ultrastable (ZnO) polymer core-shell nanoparticles with strong blue fluorescence. Adv Mater 18: 748-751.

2. Xiong HM, Xu Y, Ren QG, Xia YY (2008) Stable aqueous ZnO@polymer core-shell nanoparticles with tunable photoluminescence and their application in cell imaging. J Am Chem Soc 130: 7522-7523.

3. Subramanian V, Wolf EE, Kamat PV (2003) Green emission to probe photoinduced charging events in ZnO-Au nanoparticles. Charge distribution and Fermi-level equilibration. J Phys Chem B 107: 7479-7485.

4. Hung WS, Lin JT, Chien CH, Tao T, Sun SS, et al. (2004) Highly phosphorescent bis-cyclometalated iridium complexes containing benzoimidazole-based ligands. Chem Mater 16: 2480-2488.

5. Nakashima K (2003) Lophine derivatives as versatile analytical tools. Biomed Chromatogr 17: 83-95.

6. Wiseman A (1985) Handbook of Enzyme Biotechnology, Horwoodi, Chichester.

7. Masuda Y, Kato K (2008) High c-axis oriented stand-alone ZnO self-assembled film. Crystal Growth and Design 8: 275-279.

8. Zhang XM, Lu MY, Zhang Y, Chen LJ, Wang ZL, et al. (2009) Fabrication of a high-brightness blue-light-emitting diode using a ZnO-nanowire array grown on p-GaN thin film. Adv Mater 21: 2767-2770.

9. Topoglidis E, Cass AEG, Regan BO, Durrant JR (2001) Immobilisation and bioelectrochemistry of proteins on nanoporous TiO_2 and ZnO films. J Electroanal Chem 517: 20-27.

10. Chen S, Ingram RS, Hostetler MJ, Pietron JJ (1998) Gold nanoelectrodes of varied size: Transition to molecule-like charging. Science 280: 2098-2101.

11. Ozgur U, Alivov I, Liu C, Teke A (2005) A comprehensive review of ZnO materials and devices. J Appl Phys 98: pp:041301.

12. Huang MH, Mao S, Feick H, Yan HQ (2001) Room-temperature ultraviolet nanowire nanolasers. Science 292: 1897-1899.

13. Wang YW, Zhang LD, Wang GZ (2002) Catalytic growth of semiconducting zinc oxide nanowires and their photoluminescence properties. J Cryst Growth 234: 171-175.

14. Feng X, Feng L, Jin M, Zhai J (2004) Reversible super-hydrophobicity to super-hydrophilicity transition of aligned ZnO nanorod films. J Am Chem Soc 126: 62-63.

15. Law M, Greene LE, Jhonson JC (2005) Nanowire dye-sensitized solar cells. Nat Mater 4: 455-459.

16. Karunakaran C, Jayabharathi J, Kalaiarasi V, Jayamoorthy K (2014) Characterization and electronic spectral studies of 2-(naphthalen-1-yl)-4,5-diphenyl-1H-imidazole bound Fe_2O_3 nanoparticles. Spectrochimica Acta Part A 120: 84-87.

17. Wang X, Zhang Q, Wan Q, Dai G (2011) Controllable ZnO architectures by ethanolamine-assisted hydrothermal reaction for enhanced photocatalytic activity. J Phys Chem C 115: 2769-2775.

18. Becker J, Raghupathi KR, Pierre J (2011) Tuning of the crystallite and particle sizes of ZnO nanocrystalline materials in solvothermal synthesis and their photocatalytic activity for dye degradation. J Phys Chem C 115: 13844-13850.

19. Jing L, Qu Y, Wang B, Li S (2006) Review of photoluminescence performance of nano-sized semiconductor materials and its relationships with photocatalytic activity. J Sun Sol Energy Mater Sol Cells 90: 1773-1787.

20. Hou J, Huo L, He C, Yang C (2006) Synthesis and absorption spectra of Poly (3-(phenylenevinyl) thiophene)s with conjugated side chains. Macromolecules 39: 594-603.

21. He WY, Li Y, Xue C, Hu ZD (2005) Effect of Chinese medicine alpinetin on the structure of human serum albumin. Bioorg Med Chem 13: 1837-1845.

22. Kavarnos GJ, Turro N (1986) Photosensitization by reversible electron transfer: Theories, experimental evidence, and examples. Chem Rev 86: 401-449.